Finite Element Simulation of Forced Convection in a Flat Plate Solar Collector: Influence of Nanofluid with Double Nanoparticles

R. Nasrin[†] and M. A. Alim

Department of Mathematics, Bangladesh University of Engineering & Technology, Dhaka-1000, Bangladesh.

[†] Corresponding Author Email: *rehena@math.buet.ac.bd*

ABSTRACT

This work compares heat loss characteristics across a riser pipe of a flat plate solar collector filled water based nanofluid of double nanoparticles (alumina and copper) with single nanoparticle (alumina). Also this study compares heat transfer phenomena among four nanofluids namely water-copper oxide, water-alumina, water-copper and water-silver nanofluids. Comparisons are obtained by numerically solving assisted convective heat transfer problem of a cross section of flat plate solar collector. Governing partial differential equations are solved using the finite element simulation with Galerkin's weighted residual technique. The average Nusselt number (Nu) at the top hot wall, average temperature (θ_{av}), mean velocity (V_{av}), percentage of collector efficiency (η), mid-height dimensional temperature (T) for both nanofluid and base fluid through the collector pipe are presented graphically. The results show that the better performance of heat loss through the riser pipe of the flat plate solar collector is found by using the double nanoparticles (alumina and copper) than single nanoparticle (only alumina). When comparing the four nanofluids considering the same solid volume fraction ($\phi = 5\%$), this study claims that the average Nusselt number for water-Ag nanofluid is higher than others.

Keywords: Forced convection, Flat plate solar collector, Finite element simulation, Nanofluids, Nanoparticles, Solid volume fraction.

NOMENCLATURE

A	surface area of the collector (m^2)	x, y	dimensional coordinates (m)
C_p	specific heat at constant pressure (J kg^{-1} K^{-1})	**Greek Symbols**	
h	local heat transfer coefficient (W m^{-2} K^{-1})	α	fluid thermal diffusivity (m^2 s^{-1})
I	intensity of solar radiation (W m^{-2}),	β	thermal expansion coefficient (K^{-1})
k	thermal conductivity (W m^{-1} K^{-1})	φ	nanoparticles volume fraction
L	length of the riser pipe (m)	ν	kinematic viscosity (m^2 s^{-1})
m	mass flow rate (Kg s^{-1})	η	collector efficiency
Nu	Nusselt number, $Nu = hL/k_f$	θ	dimensionless temperature,
Pr	Prandtl number,	ρ	density (kg m^{-3})
Re	Reynolds number,	μ	dynamic viscosity (N s m^{-2})
T	dimensional temperature (K)	V	dimensionless velocity field
T_{in}	input temperature of fluid (K)	**Subscripts**	
T_{out}	output temperature of fluid (K)	av	average
u, v	dimensional x and y components of velocity (m s^{-1})	col	collector
		f	fluid
U, V	dimensionless velocities	nf	nanofluid
U_i	input velocity of fluid (ms^{-1})	s	solid particle
X, Y	dimensionless coordinates	1	alumina nanoparticle
		2	copper nanoparticle

1. INTRODUCTION

The fluids with solid-sized nanoparticles suspended in them are called "nanofluids." Applications of nanoparticles in thermal field are to enhance heat transfer from solar collectors to storage tanks, to improve efficiency of coolants in transformers. The flat-plate solar collector is commonly used today for the collection of low temperature solar thermal energy. It is used for solar water-heating systems in homes and solar space heating. Because of the desirable environmental and safety aspects it is widely believed that solar energy should be utilized instead of other alternative energy forms, even when the costs involved are slightly higher. Solar collectors are key elements in many applications, such as building heating systems, solar drying devices, etc. Solar energy has the greatest potential of all the sources of renewable energy especially when other sources in the country have depleted. Forced convection is a mechanism in which fluid motion is generated by an external source (like a pump, fan, suction device etc.). Significant amounts of heat energy can be transported very efficiently by this system and it is found very commonly in everyday life, including central heating, air conditioning, steam turbines and in many other machines

Lund (1986) analyzed general thermal behavior of parallel-flow flat-plate solar collector absorbers. Nag *et al*. (1989) analyzed parametric study of parallel flow flat plate solar collector using finite element method. Piao *et al*. (1994) studied forced convective heat transfer in cross-corrugated solar air heaters. Kolb *et al*. (1999) experimentally studied solar air collector with metal matrix absorber. Tripanagnostopoulos *et al*. (2000) investigated solar collectors with colored absorbers. Kazeminejad (2002) numerically analyzed two dimensional parallel flow flat-plate solar collectors. Temperature distribution over the absorber plate of a parallel flow flat-plate solar collector was analyzed with one- and two-dimensional steady-state conduction equations with heat generations. Generally a direct absorption solar collector (DAC) using nanofluids as the working fluid performs better than a flat-plate collector. Much better designed flat-plate collectors might be able to match a nanofluid based DAC under certain conditions. Lambert *et al*. (2006) conducted Enhanced heat transfer using oscillatory flows in solar collectors. They proposed the use of oscillatory laminar flows to enhance the transfer of heat from solar collectors.

Struckmann (2008) analyzed flat-plate solar collector where efforts had been made to combine a number of the most important factors into a single equation and thus formulate a mathematical model which would describe the thermal performance of the collector in a computationally efficient manner. Natarajan and Sathish (2009) studied role of nanofluids in solar water heater. Heat transfer enhancement in solar devices is one of the key issues of energy saving and compact designs. The aim of this paper was to analyze and compare the heat transfer properties of the nanofluids with the conventional fluids. Tyagi *et al*. (2009) investigated Predicted efficiency of a low-temperature nanofluid- based direct absorption solar collector. It was observed that the presence of nanoparticles increased the absorption of incident radiation by more than nine times over that of pure water. Azad (2009) investigated interconnected heat pipe solar collector. Performance of a prototype of the heat pipe solar collector was experimentally examined and the results were compared with those obtained through theoretical analysis. Iordanou (2009) investigated flat-plate solar collectors for water heating with improved heat Transfer for application in climatic conditions of the mediterranean region. The aim of this research project was to improve the thermal performance of passive flat plate solar collectors using a novel cost effective enhanced heat transfer technique.

Álvarez *et al*. (2010) studied finite element modelling of a solar collector. A mathematical model of a serpentine flat-plate solar collector using finite elements was presented. The numerical simulations focused on the thermal and hydrodynamic behavior of the collector. Otanicar *et al*. (2010) studied nanofluid-based direct absorption solar collector. They reported on the experimental results on solar collectors based on nanofluids made from a variety of nanoparticles carbon nanotubes, graphite, and silver. They demonstrated efficiency improvements of up to 5% in solar thermal collectors by utilizing nanofluids as the absorption mechanism. In addition the experimental data were compared with a numerical model of a solar collector with direct absorption nanofluids. Karanth *et al*. (2011) performed numerical simulation of a solar flat plate collector using discrete transfer radiation model (DTRM)–a CFD Approach. Dynamics (CFD) by employing conjugate heat transfer showed that the heat transfer simulation due to solar irradiation to the fluid medium, increased with an increase in the mass flow rate. Zambolin (2011) theoretically and experimentally performed solar thermal collector systems and components. Testing of thermal efficiency and optimization of these solar thermal collectors were addressed and discussed in this work. Enhancement of flat-plate solar collector thermal performance with silver nano-fluid was conducted by Polvongsri and Kiatsiriroat (2011). With higher thermal conductivity of the working fluid the solar collector performance could be enhanced compared with that of water. The solar collector efficiency with the nano-fluid was still high even the inlet temperature of the working fluid was increased. Martín *et al*. (2011) also analyzed experimental heat transfer research in enhanced flat-plate solar collectors. To test the enhanced solar collector and compare with a standard one, an experimental side-by-side solar collector test bed was designed and constructed. Taylor *et al*. (2011) analyzed nanofluid optical property characterization: towards efficient direct absorption solar collectors. Their study compared model predictions to spectroscopic measurements of extinction coefficients over wavelengths that were important for solar energy (0.25 to 2.5 μm).

Modeling of flat-plate solar collector operation in transient states was conducted by Saleh (2012). This study presents a one-dimensional mathematical model for simulating the transient processes which occur in liquid flat-plate solar collectors. The proposed model simulated the complete solar collector system including the flat-plate and the storage tank. Karuppa *et al.* (2012) experimentally investigated a new solar flat plate collector. Experiments had been carried out to test the performance of both the water heaters under water circulation with a small pump and the results were compared. The results showed that the system could reach satisfactory levels of efficiency. Amrutkar *et al.* (2012) studied solar flat plate collector analysis. It was expected that with the same collector space higher thermal efficiency or higher water temperature could be obtained.

Sandhu (2013) experimentally studied temperature field in flat-plate collector and heat transfer enhancement with the use of insert devices. Various new configurations of the conventional insert devices were tested over a wide range of Reynolds number (200-8000). Mahian *et al.* (2013) performed a review of the applications of nanofluids in solar energy. The effects of nanofluids on the performance of solar collectors and solar water heaters from the efficiency, economic and environmental considerations viewpoints and the challenges of using nanofluids in solar energy devices were discussed. Dara *et al.* (2013) conducted evaluation of a passive flat-plate solar collector. The research investigated the variations of top loss heat transfer coefficient with absorber plate emittance; and air gap spacing between the absorber plate and the cover plate. Rao *et al.* (2013) analyzed finite element technique of radiation and mass transfer flow past semi- infinite moving vertical plate with viscous dissipation. Their result showed that increased cooling (Gr>0) of the plate and the Eckert number lead to a rise in the velocity. Habib and El-Zahar (2013) mathematically modeled heat-transfer for a moving sheet in a moving fluid where the heat transfer depended on the relative velocity between the moving fluid and the moving sheet to a certain value after that value the relative velocity had no effect. Effects of radiation and cold wall temperature boundary conditions on natural convection in a vertical annular porous medium were conducted by Patil *et al.* (2013). The results revealed that the Nusselt number and Sherwood number at cold wall decreased with the increase in radius ratio, whereas they increased with the radius ratio at hot wall for different temperature boundary conditions at the cold wall. Singh *et al.* (2013) studied effect of cooling system design on engine oil temperature. A simple experimental setup was developed for optimization of the centrifugal fan. It was observed that the reduction in engine oil temperature could be achieved by systematic design changes. Chabane *et al.* (2013) studied thermal performance optimization of a flat plate solar air heater. Experimentally investigates of single pass solar air heater without fins; present the aims to review of

designed and analyzed a thermal efficiency of flat-plate solar air heaters.

Nasrin and Alim (2013) investigated free convective analysis in a solar collector where the numerical results showed that the highest heat transfer rate was observed for both the largest *Pr* and *Ra*. Ghasemi and Razavi (2013) numerically conducted nanofluid simulation with finite volume Lattice-Boltzmann enhanced approach. In this paper the numerical approach was based on a modified and robust finite volume method. Kumar (2013) studied radiative heat transfer with MHD free convection flow over a stretching porous sheet in presence of heat source subjected to power law heat flux. The author discussed the effects of the various parameters entering into the problem on the temperature distribution and wall temperature gradient.

In the light of above discussions, it is seen that there has been a good number of works in the field of heat loss system through a flat plate solar collector. In spite of that there is some scope to work with fluid flow, heat loss and enhancement of collector efficiency using nanofluid. Also temperature, streamfunction and heatfunction profiles through the riser pipe of the collector can't be shown in any experimental works. In this paper, finite element simulation of heat transfer by nanofluids through the riser pipe of a flat plate solar collector is performed. The objective of this paper is to present temperature, streamfunction and heatfunction profile as well as heat loss system with the comparison of nanofluid having double nanoparticles with single nanoparticle and four different water based nanofluids.
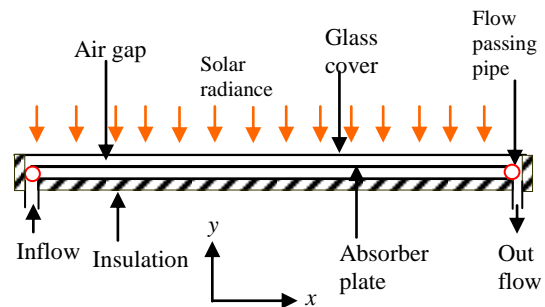
2. PROBLEM FORMULATION

Fig. 1. Schematic diagram of the solar

A cross section of the system considered in the present study is shown in Fig. 1. The system consists of a flat plate solar collector. The fluid through the copper riser pipe is water-based nanofluids. The nanofluid is assumed incompressible and the flow is considered to be laminar. It is taken that water and nanoparticles are in thermal equilibrium and no slip occurs between them. The flat-plate solar collector is an insulated metal box with a glass cover (called the glazing) and a dark-colored absorber plate. *A*, *L* and *D* are the surface area of the collector, length and inner diameter of the riser pipe. The density of the

nanofluid is approximated by the Boussinesq model. Only steady state case is considered. The computation domain is a fluid passing copper riser pipe which is attached ultrasonically to the absorber plate. The fluid enters from the left inlet and getting heat form upper and lower boundaries and finally exits from the right inlet of the riser pipe of a flat plate solar collector.

3. MATHEMATICAL FORMULATION

It is necessary to measure its thermal performance, i.e. the useful energy gain or the collector efficiency. If I is the intensity of solar radiation, incident on the aperture plane of the solar collector having a collector surface area of A, then the amount of solar radiation received by the collector is:

$$Q_i = I.A \tag{1}$$

However, a part of this radiation is reflected back to the sky, another component is absorbed by the glazing and the rest is transmitted through the glazing and reaches the absorber plate as short wave radiation. Therefore the conversion factor indicates the percentage of the solar rays penetrating the transparent cover of the collector (transmission) and the percentage being absorbed. Basically, it is the product of the rate of transmission of the cover (λ) and the absorption rate of the absorber (κ). Thus:

$$Q_{recv} = I(\lambda\kappa)A \tag{2}$$

As the collector absorbs heat its temperature is getting higher than that of the surrounding and heat is lost to the atmosphere by convection and radiation. The rate of heat loss (Q_{loss}) depends on the collector overall heat transfer coefficient (h) and the collector temperature:

$$Q_{loss} = hA(T_{col} - T_{amb}) \tag{3}$$

Thus, the rate of useful energy extracted by the collector (Q_{usfl}), expressed as a rate of extraction under steady state conditions, is proportional to the rate of useful energy absorbed by the collector, less the amount lost by the collector to its surroundings. This is expressed as:

$$Q_{usfl} = Q_{recv} - Q_{loss} = I(\lambda\kappa)A - hA(T_{col} - T_{amb}) \tag{4}$$

where T_{col} and T_{amb} are collector temperature and ambient temperature outside the collector respectively. It is also known that the rate of extraction of heat from the collector may be measured by means of the amount of heat carried away in the fluid passed through it, which is:

$$Q_{usfl} = mC_p(T_{out} - T_{in}) \tag{5}$$

Equation (4) may be inconvenient because of the difficulty in defining the collector average temperature. It is convenient to define a quantity that relates the actual useful energy gain of a collector to the useful gain if the whole collector surface were at the fluid mean temperature. This quantity is known as "the collector heat removal factor (F_R)" and is expressed as:

$$F_R = \frac{mC_p(T_{out} - T_{in})}{A\left[I(\lambda\kappa) - h(T_m - T_{amb})\right]} \tag{6}$$

where T_{in}, T_{out} and $T_m = \dfrac{T_{out} + T_{in}}{2}$ are inlet, outlet and fluid mean temperatures, respectively.

The maximum possible useful energy gain in a solar collector occurs when the whole collector is at the inlet fluid temperature. The actual useful energy gain (Q_{usfl}), is found by multiplying the collector heat removal factor (F_R) by the maximum possible useful energy gain. This allows the rewriting of Eq (4):

$$Q_{usfl} = F_R A\left[I(\lambda\kappa) - h(T_m - T_{amb})\right] \tag{7}$$

Equation (7) is a widely used relationship for measuring collector energy gain and is generally known as the "Hottel-Whillier-Bliss equation".

A measure of a flat plate collector performance is the collector efficiency (η) defined as the ratio of the useful energy gain (Q_{usfl}) to the incident solar energy.

$$\eta = \frac{\text{useful gain}}{\text{available energy}} = \frac{mC_p(T_{out} - T_{in})}{AI} \tag{8}$$

The instantaneous thermal efficiency of the collector is:

$$\eta = \frac{Q_{usfl}}{A\ I} = \frac{F_R A\ \left[I(\lambda\kappa) - h(T_m - T_{amb})\right]}{AI}$$
$$= F_R(\lambda\kappa) - F_R h \frac{(T_m - T_{amb})}{I} \tag{9}$$

where m is the mass flow rate of the fluid flowing through the collector; C_p is the specific heat at constant pressure.

The governing equations for laminar forced convection through a solar collector filled with water-alumina nanofluid in terms of the Navier-Stokes and energy equation (dimensional form) are given as:

$$\frac{\partial u}{\partial x} + \frac{\partial v}{\partial y} = 0 \tag{10}$$

$$\rho_{nf}\left(u\frac{\partial u}{\partial x} + v\frac{\partial u}{\partial y}\right) = -\frac{\partial p}{\partial x} + \mu_{nf}\left(\frac{\partial^2 u}{\partial x^2} + \frac{\partial^2 u}{\partial y^2}\right) \tag{11}$$

$$\rho_{nf}\left(u\frac{\partial v}{\partial x} + v\frac{\partial v}{\partial y}\right) = -\frac{\partial p}{\partial y} + \mu_{nf}\left(\frac{\partial^2 v}{\partial x^2} + \frac{\partial^2 v}{\partial y^2}\right) \tag{12}$$

$$u\frac{\partial T}{\partial x} + v\frac{\partial T}{\partial y} = \alpha_{nf}\left(\frac{\partial^2 T}{\partial x^2} + \frac{\partial^2 T}{\partial y^2}\right) \tag{13}$$

The thermal diffusivity:

$$\alpha_{nf} = k_{nf}\big/\left(\rho C_p\right)_{nf} \tag{14}$$

the density :

$$\rho_{nf} = (1-\phi)\rho_f + \phi\rho_s \qquad (15)$$

the heat capacitance:

$$\left(\rho C_p\right)_{nf} = (1-\phi)\left(\rho C_p\right)_f + \phi\left(\rho C_p\right)_s \qquad (16)$$

the viscosity of the nanofluid is considered by the Pak and Cho correlation (1998). This correlation is given as:

$$\mu_{nf} = \mu_f \left(1 + 39.11\phi + 533.9\phi^2\right) \qquad (17)$$

the thermal conductivity of Maxwell Garnett (MG) model (1904) is :

$$k_{nf} = k_f \frac{k_s + 2k_f - 2\phi\left(k_f - k_s\right)}{k_s + 2k_f + \phi\left(k_f - k_s\right)} \qquad (18)$$

For water based nanofluid with double nanoparticles the modified properties of Eqs. (15 to 18) are as follows:

$$\rho_{nf} = (1-\phi_1-\phi_2)\rho_f + \left(\phi_1\rho_{s1} + \phi_2\rho_{s2}\right) \qquad (15^/)$$

is the density:

$$\left(\rho C_p\right)_{nf} = (1-\phi_1-\phi_2)\left(\rho C_p\right)_f + \phi_1\left(\rho C_p\right)_{s1} + \phi_2\left(\rho C_p\right)_{s2} \qquad (16^/)$$

is the heat capacitance.

The effective viscosity of the nanofluid is considered by the Pak and Cho correlation (1998). This correlation is given as modified form

$$\mu_{nf} = \mu_f \left\{1 + 39.11\left(\phi_1 + \phi_2\right) + 533.9\left(\phi_1^2 + \phi_2^2\right)\right\} \qquad (17^/)$$

Also the effective thermal conductivity (modified form) is used from Maxwell Garnett (1904) model

$$k_{nf} = k_f \frac{\left(k_{s1}+k_{s2}\right) + 2k_f - 2\phi_1\left(k_f - k_{s1}\right) - 2\phi_2\left(k_f - k_{s2}\right)}{\left(k_{s1}+k_{s2}\right) + 2k_f + \phi_1\left(k_f - k_{s1}\right) + \phi_2\left(k_f - k_{s2}\right)} \qquad (18^/)$$

Where subscripts 1 and 2 represent alumina and copper nanoparticles respectively.

The boundary conditions are:

At all solid boundaries: $u = v = 0$

At the top and bottom surfaces of the pipe: heat flux per unit area $-k_{nf}\dfrac{\partial T}{\partial y} = q = I(\lambda\kappa) - h(T_{col} - T_{amb})$

At the inlet boundary: $T = T_{in}$, $u = U_{in}$

At the outlet boundary: convective boundary condition $p = 0$

The above equations are non-dimensionalized by using the following dimensionless dependent and independent variables:

$$X = \frac{x}{L}, Y = \frac{y}{L}, U = \frac{u}{U_{in}}, V = \frac{v}{U_{in}}, P = \frac{p}{\rho_f U_{in}^2},$$

$$\theta = \frac{(T - T_{in})k_f}{qL}$$

Then the non-dimensional governing equations are

$$\frac{\partial U}{\partial X} + \frac{\partial V}{\partial Y} = 0 \qquad (19)$$

$$U\frac{\partial U}{\partial X} + V\frac{\partial U}{\partial Y} = -\frac{\rho_f}{\rho_{nf}}\frac{\partial P}{\partial X} + \frac{\nu_{nf}}{\nu_f}\frac{1}{Re}\left(\frac{\partial^2 U}{\partial X^2} + \frac{\partial^2 U}{\partial Y^2}\right) \qquad (20)$$

$$U\frac{\partial V}{\partial X} + V\frac{\partial V}{\partial Y} = -\frac{\rho_f}{\rho_{nf}}\frac{\partial P}{\partial Y} + \frac{\nu_{nf}}{\nu_f}\frac{1}{Re}\left(\frac{\partial^2 V}{\partial X^2} + \frac{\partial^2 V}{\partial Y^2}\right) \qquad (21)$$

$$U\frac{\partial \theta}{\partial X} + V\frac{\partial \theta}{\partial Y} = \frac{1}{RePr}\frac{\alpha_{nf}}{\alpha_f}\left(\frac{\partial^2 \theta}{\partial X^2} + \frac{\partial^2 \theta}{\partial Y^2}\right) \qquad (22)$$

where $Pr = \dfrac{\nu_f}{\alpha_f}$ is the Prandtl number, $Re = \dfrac{U_{in}L}{\nu_f}$ is the Reynolds number.The corresponding boundary conditions take the following form:

At all solid boundaries: $U = V = 0$

At the upper and lower walls: $\dfrac{\partial \theta}{\partial Y} = -\dfrac{k_f}{k_{nf}}$

At the inlet boundary: $\theta = 0$, $U = 1$

At the outlet boundary: convective boundary condition $P = 0$

3.1 Mean Nusselt Number

The average Nusselt number (Nu) is expected to depend on a number of factors such as thermal conductivity, heat capacitance, viscosity, flow structure of nanofluids, volume fraction, dimensions and fractal distributions of nanoparticles. The rate of heat transfer along the upper heated wall of the collector is used by Saleh et al. (2011) as

$$Nu = -\int_0^1 \frac{k_{nf}}{k_f}\frac{\partial \theta}{\partial Y} dX \qquad (23)$$

3.2 Mean Temperature and Velocity

The mean bulk temperature and average sub domain velocity of the fluid inside the collector may be written as $\theta_{av} = \int \theta\, d\bar{V}/\bar{V}$ and $V_{av} = \int V\, d\bar{V}/\bar{V}$, where $\bar{V}$ is the volume of the collector.

3.3 Streamfunction

Streamfunction ψ is obtained from velocity components U and V. The relationship between stream function and velocity components is

$$U = \frac{\partial \psi}{\partial Y}, \quad V = -\frac{\partial \psi}{\partial X}.$$

Thus $\dfrac{\partial^2 \psi}{\partial X^2} + \dfrac{\partial^2 \psi}{\partial Y^2} = \dfrac{\partial U}{\partial Y} - \dfrac{\partial V}{\partial X}$ (24)

3.4 Heatfunction

Heatfunction ξ is obtained from conductive heat fluxes $\left(-\dfrac{\partial \theta}{\partial X}, -\dfrac{\partial \theta}{\partial Y} \right)$ as well as convective heat fluxes ($U\theta$, $V\theta$). It satisfies the steady energy balance equation such that

$$U\theta - \dfrac{\partial \theta}{\partial X} = \dfrac{\partial \xi}{\partial Y}, \quad V\theta - \dfrac{\partial \theta}{\partial Y} = -\dfrac{\partial \xi}{\partial X} \quad .$$

Thus $\dfrac{\partial^2 \xi}{\partial X^2} + \dfrac{\partial^2 \xi}{\partial Y^2} = \dfrac{\partial}{\partial Y}(U\theta) - \dfrac{\partial}{\partial X}(V\theta)$ (25)

4. NUMERICAL IMPLEMENTATION

The governing equations along with the boundary conditions are solved numerically, employing Galerkin weighted residual finite element techniques. To derive the finite element equations, the method of weighted residuals Zienkiewicz (1991) is applied to the governing Eqs (19) to (22) as

$$\int_A N_\alpha \left(\dfrac{\partial U}{\partial X} + \dfrac{\partial V}{\partial Y} \right) dA = 0 \tag{26}$$

$$\int_A N_\alpha \left(U \dfrac{\partial U}{\partial X} + V \dfrac{\partial U}{\partial Y} \right) dA = -\dfrac{\rho_f}{\rho_{nf}} \int_A H_\lambda \left(\dfrac{\partial P}{\partial X} \right) dA$$
$$+ \dfrac{1}{Re} \dfrac{\nu_{nf}}{\nu_f} \int_A N_\alpha \left(\dfrac{\partial^2 U}{\partial X^2} + \dfrac{\partial^2 U}{\partial Y^2} \right) dA \tag{27}$$

$$\int_A N_\alpha \left(U \dfrac{\partial V}{\partial X} + V \dfrac{\partial V}{\partial Y} \right) dA = -\dfrac{\rho_f}{\rho_{nf}} \int_A H_\lambda \left(\dfrac{\partial P}{\partial X} \right) dA$$
$$+ \dfrac{1}{Re} \dfrac{\nu_{nf}}{\nu_f} \int_A N_\alpha \left(\dfrac{\partial^2 V}{\partial X^2} + \dfrac{\partial^2 V}{\partial Y^2} \right) dA \tag{28}$$

$$\int_A N_\alpha \left(U \dfrac{\partial \theta}{\partial X} + V \dfrac{\partial \theta}{\partial Y} \right) dA = \dfrac{\alpha_{nf}}{RePr\alpha_f} \int_A N_\alpha \left(\dfrac{\partial^2 \theta}{\partial X^2} + \dfrac{\partial^2 \theta}{\partial Y^2} \right) dA \tag{29}$$

where A is the element area, N_α (α = 1, 2, … … , 6) are the element interpolation functions for the velocity components and the temperature and H_λ (λ = 1, 2, 3) are the element interpolation functions for the pressure.

Applying Gauss's Divergence theorem to the 2nd ordered derivative part of the governing equations :

$$\int_A \nabla \cdot \mathbf{F} \, dA = \int_c \mathbf{F} \cdot \mathbf{n} \, ds$$

$$\Rightarrow \int_A \nabla \cdot (N_\alpha \, \nabla u) dA = \int_c (N_\alpha \, \nabla u) \cdot \mathbf{n} \, ds$$

$$\Rightarrow \int_A N_\alpha \nabla \cdot \nabla u \, dA + \int_A \nabla N_\alpha \cdot \nabla u \, dA = \int_c N_\alpha \, \nabla u \cdot \mathbf{n} \, ds$$

using $\nabla \cdot (\phi \mathbf{F}) = \phi \nabla \cdot \mathbf{F} + \nabla \phi . \mathbf{F}$

Thus 2nd ordered terms in momentum and energy Eqs (27) to (29) can be written as

$$\int_A N_\alpha \left(\dfrac{\partial^2 U}{\partial X^2} + \dfrac{\partial^2 U}{\partial Y^2} \right) dA = -\int_A \left(\dfrac{\partial N_\alpha}{\partial X} \dfrac{\partial U}{\partial X} + \dfrac{\partial N_\alpha}{\partial Y} \dfrac{\partial U}{\partial Y} \right)$$
$$+ \int_{S_0} N_\alpha S_x dS_0$$

$$\int_A N_\alpha \left(\dfrac{\partial^2 V}{\partial X^2} + \dfrac{\partial^2 V}{\partial Y^2} \right) dA = -\int_A \left(\dfrac{\partial N_\alpha}{\partial X} \dfrac{\partial V}{\partial X} + \dfrac{\partial N_\alpha}{\partial Y} \dfrac{\partial V}{\partial Y} \right) dA$$
$$+ \int_{S_0} N_\alpha S_x dS_0$$

$$\int_A N_\alpha \left(\dfrac{\partial^2 \theta}{\partial X^2} + \dfrac{\partial^2 \theta}{\partial Y^2} \right) dA = -\int_A \left(\dfrac{\partial N_\alpha}{\partial X} \dfrac{\partial \theta}{\partial X} + \dfrac{\partial N_\alpha}{\partial Y} \dfrac{\partial \theta}{\partial Y} \right) dA$$
$$+ \int_{S_w} N_\alpha q_w dS_w$$

where surface tractions (S_x, S_y) along outflow boundary S_0 and velocity components and fluid temperature or heat flux (q_w) that flows into or out from domain along wall boundary S_w.

Applying Gaussian quadrature technique to momentum and energy equations in order to generate the boundary integral terms associated with the surface tractions and heat flux

$$\int_A N_\alpha \left(U \dfrac{\partial U}{\partial X} + V \dfrac{\partial U}{\partial Y} \right) dA + \dfrac{\rho_f}{\rho_{nf}} \int_A H_\lambda \left(\dfrac{\partial P}{\partial X} \right) dA +$$
$$\dfrac{1}{Re} \dfrac{\nu_{nf}}{\nu_f} \int_A \left(\dfrac{\partial N_\alpha}{\partial X} \dfrac{\partial U}{\partial X} + \dfrac{\partial N_\alpha}{\partial Y} \dfrac{\partial U}{\partial Y} \right) dA = \int_{S_0} N_\alpha S_x dS_0 \tag{30}$$

$$\int_A N_\alpha \left(U \dfrac{\partial V}{\partial X} + V \dfrac{\partial V}{\partial Y} \right) dA + \dfrac{\rho_f}{\rho_{nf}} \int_A H_\lambda \left(\dfrac{\partial P}{\partial Y} \right) dA +$$
$$\dfrac{1}{Re} \dfrac{\nu_{nf}}{\nu_f} \int_A \left(\dfrac{\partial N_\alpha}{\partial X} \dfrac{\partial V}{\partial X} + \dfrac{\partial N_\alpha}{\partial Y} \dfrac{\partial V}{\partial Y} \right) dA = \int_{S_0} N_\alpha S_y dS_0 \tag{31}$$

$$\int_A N_\alpha \left(U \dfrac{\partial T}{\partial X} + V \dfrac{\partial T}{\partial Y} \right) dA + \dfrac{1}{RePr} \dfrac{\alpha_{nf}}{\alpha_f}$$
$$\int_A \left(\dfrac{\partial N_\alpha}{\partial X} \dfrac{\partial T}{\partial X} + \dfrac{\partial N_\alpha}{\partial Y} \dfrac{\partial T}{\partial Y} \right) dA = \int_{S_w} N_\alpha q_w dS_w \tag{32}$$

The basic unknowns for the above differential equations are the velocity components U, V the temperature θ and the pressure P. The six node triangular element is used in this work for the development of the finite element equations. All six

nodes are associated with velocities as well as temperature. Only the corner nodes are associated with pressure. This means that a lower order polynomial is chosen for pressure and which is satisfied through continuity equation. The Galerkin finite element method Taylor and Hood (1973) and Dechaumphai (1999) is used to solve velocity components and the temperature distribution and linear interpolation for the pressure distribution according to their highest derivative orders in the differential Eqs (26), (30 to 32) are as

$$U(X,Y) = N_\beta U_\beta , V(X,Y) = N_\beta V_\beta ,$$
$$T(X,Y) = N_\beta T_\beta \text{ and } P(X,Y) = H_\lambda P_\lambda$$

where $\beta = 1, 2, \ldots \ldots , 6$ and $\lambda = 1, 2, 3$. Thus

$$U_\beta \int_A N_\alpha N_{\beta,x} \, dA + V_\beta \int_A N_\alpha N_{\beta,y} \, dA = 0 \tag{33}$$

$$U_\beta U_\gamma \int_A N_\alpha N_\beta N_{\gamma,x} \, dA + V_\beta U_\gamma \int_A N_\alpha N_\beta N_{\gamma,y} \, dA$$
$$+ \frac{1}{Re} \frac{\nu_{nf}}{\nu_f} U_\beta \left(\int_A N_{\alpha,x} N_{\beta,x} dA + \int_A N_{\alpha,y} N_{\beta,y} dA \right)$$
$$+ \frac{\rho_f}{\rho_{nf}} P_\mu \int_A H_\lambda H_{\mu,x} \, dA = \int_{S_0} N_\alpha S_x dS_0 \tag{34}$$

$$U_\beta V_\gamma \int_A N_\alpha N_\beta N_{\gamma,x} \, dA + V_\beta V_\gamma \int_A N_\alpha N_\beta N_{\gamma,y} \, dA +$$
$$\frac{1}{Re} \frac{\nu_{nf}}{\nu_f} V_\beta \left(\int_A N_{\alpha,x} N_{\beta,x} dA + \int_A N_{\alpha,y} N_{\beta,y} dA \right) +$$
$$\frac{\rho_f}{\rho_{nf}} P_\mu \int_A H_\lambda H_{\mu,y} \, dA = \int_{S_0} N_\alpha S_y dS_0 \tag{35}$$

$$U_\beta \theta_\gamma \int_A N_\alpha N_\beta N_{\gamma,x} \, dA + V_\beta \theta_\gamma \int_A N_\alpha N_\beta N_{\gamma,y} \, dA +$$
$$\frac{1}{RePr} \frac{\alpha_{nf}}{\alpha_f} \theta_\beta \left(\int_A N_{\alpha,x} N_{\beta,x} dA + \int_A N_{\alpha,y} N_{\beta,y} dA \right)$$
$$= \int_{S_w} N_\alpha q_w dS_w \tag{36}$$

The coefficients in above governing equations are denoted as

$$K_{\alpha\beta}{}^x = \int_A N_\alpha N_{\beta,x} dA , \quad K_{\alpha\beta}{}^y = \int_A N_\alpha N_{\beta,y} dA ,$$

$$K_{\alpha\beta\gamma}{}^x = \int_A N_\alpha N_\beta N_{\gamma,x} dA$$

$$K_{\alpha\beta\gamma}{}^y = \int_A N_\alpha N_\beta N_{\gamma,y} dA , \quad K_{\alpha\beta} = \int_A N_\alpha N_\beta dA ,$$

$$S_{\alpha\beta}{}^{xx} = \int_A N_{\alpha,x} N_{\beta,x} dA$$

$$S_{\alpha\beta}{}^{yy} = \int_A N_{\alpha,y} N_{\beta,y} dA ,$$

$$M_{\lambda\mu}{}^x = \int_A H_\lambda H_{\mu,x} dA , \quad M_{\lambda\mu}{}^y = \int_A H_\lambda H_{\mu,y} dA$$

$$Q_\alpha{}^u = \int_{S_0} N_\alpha S_x dS_0 , \qquad Q_\alpha{}^v = \int_{S_0} N_\alpha S_y dS_0 ,$$
$$Q_\alpha{}^\theta = \int_{S_w} N_\alpha q_w dS_w$$

These coefficients are solved by Galerkin's weighted residual method. Substituting the element velocity components, the temperature and the pressure distributions from Eqs.(33 to 36), the linear algebraic equations are

$$K_{\alpha\beta}{}^x U_\beta + K_{\alpha\beta}{}^y V_\beta = 0 \tag{37}$$

$$K_{\alpha\beta\gamma}{}^x U_\beta U_\gamma + K_{\alpha\beta\gamma}{}^y V_\gamma U_\gamma + \frac{\rho_f}{\rho_{nf}} M_{\lambda\mu}{}^x P_\mu +$$
$$\frac{1}{Re} \frac{\nu_{nf}}{\nu_f} \left(S_{\alpha\beta}{}^{xx} + S_{\alpha\beta}{}^{yy} \right) U_\beta = Q_\alpha{}^u \tag{38}$$

$$K_{\alpha\beta\gamma}{}^x U_\beta V_\gamma + K_{\alpha\beta\gamma}{}^y V_\gamma V_\gamma + \frac{\rho_f}{\rho_{nf}} M_{\lambda\mu}{}^y P_\mu$$
$$+ \frac{1}{Re} \frac{\nu_{nf}}{\nu_f} \left(S_{\alpha\beta}{}^{xx} + S_{\alpha\beta}{}^{yy} \right) V_\beta = Q_\alpha{}^v \tag{39}$$

$$K_{\alpha\beta\gamma}{}^x U_\beta \theta_\gamma + K_{\alpha\beta\gamma}{}^y V_\beta \theta_\gamma +$$
$$\frac{1}{RePr} \frac{\alpha_{nf}}{\alpha_f} \left(S_{\alpha\beta}{}^{xx} + S_{\alpha\beta}{}^{yy} \right) \theta_\beta = Q_\alpha{}^\theta \tag{40}$$

The linear algebraic equations are solved by applying the Newton-Raphson iteration technique

$$F_\alpha{}^p = K_{\alpha\beta}{}^x U_\beta + K_{\alpha\beta}{}^y V_\beta \tag{41}$$

$$F_\alpha{}^u = K_{\alpha\beta\gamma}{}^x U_\beta U_\gamma + K_{\alpha\beta\gamma}{}^y V_\gamma U_\gamma + \frac{\rho_f}{\rho_{nf}} M_{\lambda\mu}{}^x P_\mu$$
$$+ \frac{1}{Re} \frac{\nu_{nf}}{\nu_f} (S_{\alpha\beta}{}^{xx} + S_{\alpha\beta}{}^{yy}) U_\beta - Q_\alpha{}^u \tag{42}$$

$$F_\alpha{}^v = K_{\alpha\beta\gamma}{}^x U_\beta V_\gamma + K_{\alpha\beta\gamma}{}^y V_\gamma V_\gamma + \frac{\rho_f}{\rho_{nf}} M_{\lambda\mu}{}^y P_\mu$$
$$+ \frac{1}{Re} \frac{\nu_{nf}}{\nu_f} (S_{\alpha\beta}{}^{xx} + S_{\alpha\beta}{}^{yy}) V_\beta - Q_\alpha{}^v \tag{43}$$

$$F_\alpha{}^\theta = K_{\alpha\beta\gamma}{}^x U_\beta \theta_\gamma + K_{\alpha\beta\gamma}{}^y V_\beta \theta_\gamma +$$
$$\frac{1}{RePr} \frac{\alpha_{nf}}{\alpha_f} \left(S_{\alpha\beta}{}^{xx} + S_{\alpha\beta}{}^{yy} \right) \theta_\beta - Q_\alpha{}^\theta \tag{44}$$

This leads to a set of algebraic equations with the incremental unknowns of the element nodal velocity components, temperatures, and pressures in the form,

$$\begin{bmatrix} K_{pu} & K_{pv} & 0 & 0 \\ K_{uu} & K_{uv} & K_{u\theta} & K_{up} \\ K_{vu} & K_{vv} & K_{v\theta} & K_{vp} \\ K_{\theta u} & K_{\theta v} & K_{\theta\theta} & 0 \end{bmatrix} \begin{bmatrix} \Delta u \\ \Delta v \\ \Delta\theta \\ \Delta p \end{bmatrix} = \begin{bmatrix} F_\alpha{}^p \\ F_\alpha{}^u \\ F_\alpha{}^v \\ F_\alpha{}^\theta \end{bmatrix} ,$$

where Δ represents the vector of nodal velocities, pressure and temperature.

$$K_{uu} = K_{\alpha\beta\gamma}xU\beta + K_{\alpha\gamma\beta}xU\gamma + K_{\alpha\beta\gamma}yV\beta +$$
$$\frac{1}{Re}\frac{v_{nf}}{v_f}\left(S_{\alpha\beta}xx + S_{\alpha\beta}yy\right),$$

$$K_{uv} = K_{\alpha\beta\gamma}yU\gamma, \ K_{vu} = K_{\alpha\beta\gamma}xV\gamma,$$

$$K_{u\theta} = 0 = K_{\theta p} = K_{p\theta} = K_{pp} = K_{v\theta},$$

$$K_{up} = \frac{\rho_f}{\rho_{nf}}M_{\lambda\mu}x, \ K_{pv} = K_{\alpha\beta}y,$$

$$K_{vp} = \frac{\rho_f}{\rho_{nf}}M_{\lambda\mu}y \ \ K_{\theta v} = K_{\alpha\beta\gamma}y\theta_\gamma$$

$$K_{vv} = K_{\alpha\beta\gamma}xU\beta + K_{\alpha\gamma\beta}xV\beta + K_{\alpha\beta\gamma}yV\gamma +$$
$$\frac{1}{Re}\frac{v_{nf}}{v_f}\left(S_{\alpha\beta}xx + S_{\alpha\beta}yy\right),$$

$$K_{\theta u} = K_{\alpha\beta\gamma}x\theta_\beta, \ K_{pu} = K_{\alpha\beta}x,$$

$$K_{\theta\theta} = K_{\alpha\beta\gamma}xU\beta + K_{\alpha\beta\gamma}yV\beta +$$
$$\frac{1}{RePr}\frac{\alpha_{nf}}{\alpha_f}(S_{\alpha\beta}xx + S_{\alpha\beta}yy)$$

The iteration process is terminated if the percentage of the overall change compared to the previous iteration is less than the specified value. The convergence of solutions is assumed when the relative error for each variable between consecutive iterations is recorded below the convergence criterion ε such that $\left|\Psi^{n+1} - \Psi^n\right| < \varepsilon$, where n is number of iteration and $\Psi = U, V, \theta$. The convergence criterion was set to $\varepsilon = 10^{-4}$.

4.1 Mesh Generation

In the finite element method, the mesh generation is the technique to subdivide a domain into a set of sub-domains, called finite elements, control volume, etc. The discrete locations are defined by the numerical grid, at which the variables are to be calculated. It is basically a discrete representation of the geometric domain on which the problem is to be solved. The computational domains with irregular geometries by a collection of finite elements make the method a valuable practical tool for the solution of boundary value problems arising in various fields of engineering. Fig. 2 displays the finite element mesh of the present physical domain.

Fig. 2. Mesh generation of the riser pipe of the solar collector

4.2 Grid Independent Test

Table 1 Grid Sensitivity Check at *Pr* = 6.6, ϕ = 5% (water-alumina nanofluid) and *Re* = 600

Nodes (elements)	*Nu* Nanofluid	*Nu* Base fluid	Time (s)
506 (60)	8.12945	6.52945	226.265
1788 (240)	9.29176	7.89976	312.594
6692 (960)	10.37518	8.48701	398.157
25860 (3840)	11.05698	9.02676	485.328
101636 (15360)	11.05711	9.02688	979.377

An extensive mesh testing procedure is conducted to guarantee a grid-independent solution for *Re* = 600 and *Pr* = 6.6 in a solar collector. In the present work, we examine five different non-uniform grid systems with the following number of elements within the resolution field: 60, 240, 960, 3840 and 15360. The numerical scheme is carried out for highly precise key in the average Nusselt number for water-Al$_2$O$_3$ nanofluid (ϕ = 5%) as well as base fluid (ϕ = 0%) for the aforesaid elements to develop an understanding of the grid fineness as shown in Table 1 and Fig. 3. The scale of the average Nusselt numbers for 3840 elements shows a little difference with the results obtained for the other elements. Hence, considering the non-uniform grid system of 3840 elements is preferred for the computation
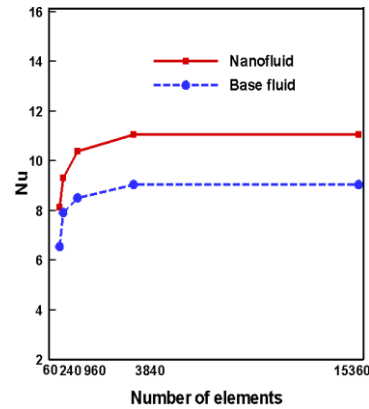

Fig. 3. Grid test for riser pipe of the solar collector

Table 2 Thermo physical properties of fluid and nanoparticles

Physical Properties	Fluid phase (Water)	Ag	Cu	Al$_2$O$_3$	CuO
C_p(J/kgK)	4179	235	385	765	535.6
ρ (kg/m^3)	997.1	10500	8933	3970	6500
k (W/mK)	0.613	429	400	40	20
$\alpha\times10^7$ (m^2/s)	1.47	1738.6	1163.1	131.7	57.45

4.3 Thermo-physical Properties

The thermo-physical properties of the nanoparticle are taken from Ogut (2009) and given in Table 2.
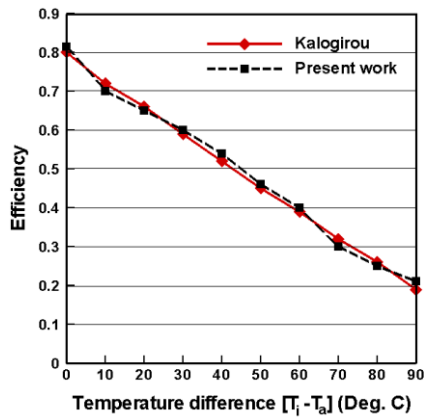
4.4 Code Validation

Fig. 4. Comparison between present code and Kalogirou (2004) at *I* = 1000 W/m²

The present numerical solution is validated by comparing the current code results for collector efficiency - temperature difference [T_i - T_a] profile of water with the graphical representation of Kalogirou (2004) for flat plate solar thermal collector at irradiation level 1000 W/m² and the mass flow rate per unit area was 0.015 (kg/s m²). Solar thermal collectors and applications were reported by Kalogirou (2004). Figure 4 demonstrates the above stated comparison. The numerical solutions (present work and Kalogirou (2004)) are in good agreement.

5. RESULTS AND DISCUSSION

In this section, numerical results of isotherms, streamlines and heatlines for various values of solid volume fraction (ϕ = ϕ_1+ϕ_2) of the water-alumina/copper nanofluid and various nanofluids such as water-CuO, water-Al₂O₃, water-Cu and water-Ag with solid volume fraction (ϕ = 5%) through a riser pipe of flat plate solar collector are displayed. The considered values of ϕ (= ϕ_1+ϕ_2) are ϕ = (1%, 3%, 5%, 7% and 10%), while the Reynolds number (*Re* = 600) and Prandtl number (*Pr* = 6.6) are chosen. In addition the values of the average Nusselt number, mean bulk temperature, mean sub domain velocity, percentage of collector efficiency and mid-height temperature (dimensional) are shown.

5.1 Effect of Double Nanoparticles

The effect of ϕ (= ϕ_1 + ϕ_2) on the thermal, velocity and heat flux fields are presented in Fig. 5 (a)-(c) while *Pr* = 6.2 and *Re* = 600. The strength of the thermal current activities is more activated with escalating volume fraction of water-Al₂O₃/Cu nanofluid. Increasing ϕ (solid volume fraction of alumina and copper nanoparticles equally), the temperature lines near the upper and lower parts of the riser pipe become flatten whereas at the lower ϕ (= 1% = 0.5% + 0.5%) they are bended due to concentration of solid particles is dominated across the pipe. With the rising values of ϕ from 1% to

5%, the temperature distributions become distorted resulting in an increase in the overall heat transfer. This result can be attributed to the dominance of the solid concentration. This is because the thermal conductivity of the solid particles is very high. This means that higher heat transfer rate is predicted by the nanofluid having two nanoparticles namely Al₂O₃ and Cu. It is worth noting that as the solid volume fraction of Al₂O₃ and Cu nanoparticles increases, the thermal boundary layer near the top and bottom surfaces of the riser pipe becomes thick which indicates a steep temperature gradients and hence, an increase in the overall heat transfer from the absorber plate containing pipe to the outlet edge. But further increasing ϕ to 10% (= 5% + 5%) there is no perturbation observed in the isothermal lines at all. Thus adding more solid volume fraction is not advantageous.

The corresponding velocity field indicates that at ϕ = 1% the velocity of nanofluid is high. Thus the nanofluid quickly passes the pipe by getting heat from upper and lower walls as a result the streamlines appear the whole riser pipe. In the velocity vector, initially the flow covers the entire domain of the pipe while it concentrates near the middle of the pipe of flat plate solar collector due to increase solid volume fraction ϕ from 1% (= 0.05% + 0.05%) to 10% (= 5% + 5%) of water-alumina/copper nanofluid. This happens because of escalating solid concentrations of flow. Nanofluid having larger density does not move freely.

The heatlines are smooth and it is observed that the lines are perfectly perpendicular to the isothermal lines and the upper and lower walls. This further indicates that the heat flow is conduction dominant. From the Fig. 5(c) it is clearly observed that the heatlines with greater strength become smaller in size at the middle of the flow pipe for ϕ = 5% (2.5%+2.5%). This happens due to more thermal conductive heat flux and as it is seen the case of the lowest solid volume fraction, the strength of heatline goes to low. The heatlines remain constant for further increasing ϕ from 5% to 10%. This means that major amount of heat flux or transport occurs for ϕ = 5% of water-Al₂O₃/Cu nanofluid.

5.2 Effect of Different Nanofluids

The performance of water and four different water based nanofluids on the dimensionless temperature, streamfunction and heatfunction are presented in Fig. 6 (a) to (c) while solid volume fraction of nanoparticles ϕ = 5%. The isotherms are smooth monotonic curves symmetric to the mid-horizontal axis. The temperature lines through the horizontal riser pipe become more heated for accordingly water, water-copper oxide, water-alumina, water-copper and water-silver. The fluid enters from the left inlet and getting heat form upper and lower boundaries and finally exits from the right inlet of the riser pipe of a flat plate solar collector. Initially (clear water) the isothermal lines are distinct through the pipe. Due to rising thermal conductivity of the nanofluid they become more heated and try to gather near the exit boundary. The thermal

boundary layer becomes thick for water-Ag nanofluid than other nanofluids and water because Ag nanoparticle has more thermal conductivity than others.
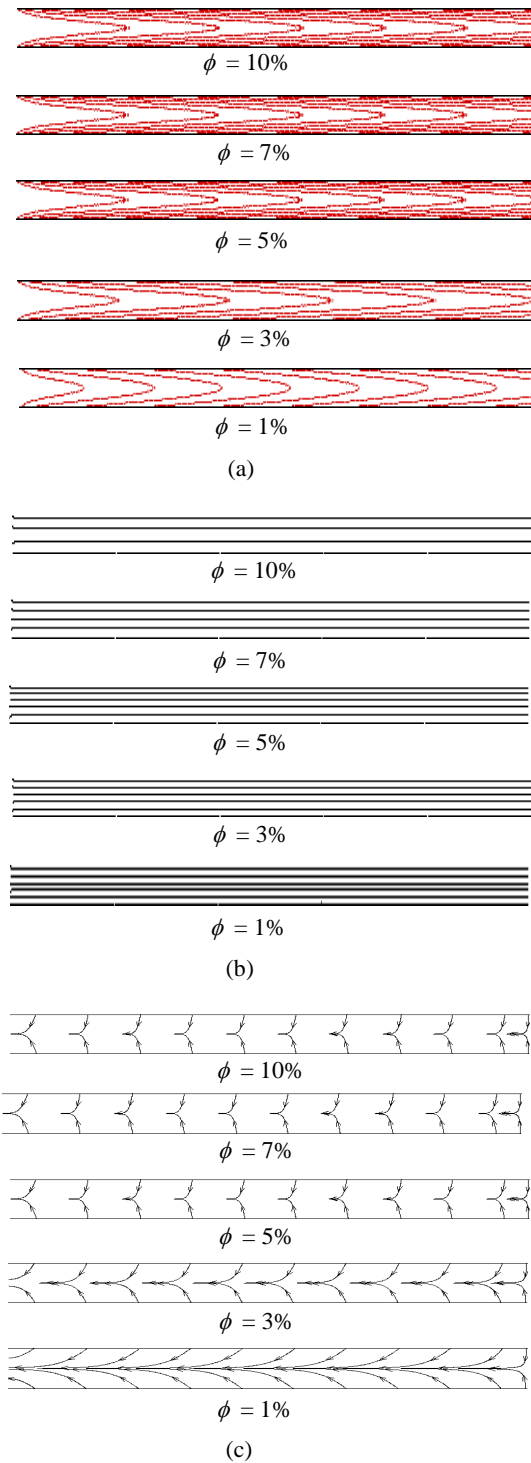

$\phi = 10\%$

$\phi = 7\%$

$\phi = 5\%$

$\phi = 3\%$

$\phi = 1\%$

(a)

$\phi = 10\%$

$\phi = 7\%$

$\phi = 5\%$

$\phi = 3\%$

$\phi = 1\%$

(b)

$\phi = 10\%$

$\phi = 7\%$

$\phi = 5\%$

$\phi = 3\%$

$\phi = 1\%$

(c)

Fig. 5. Effect of ϕ of water-alumina/copper nanofluid on (a) temperature and (b) streamfunction and (c) heatfunction

The strength of the flow circulation is much more deactivated for water, water-aluminium oxide, water-copper oxide, water-copper and water-silver

nanofluids respectively. In the velocity vector, the flow covers the whole domain of the pipe for base fluid (water) while it concentrates near the middle of the riser pipe due to rising density of the nanoparticles. Fluid with solid particles (nanofluid) has lower velocity than base fluid (without solid particle).
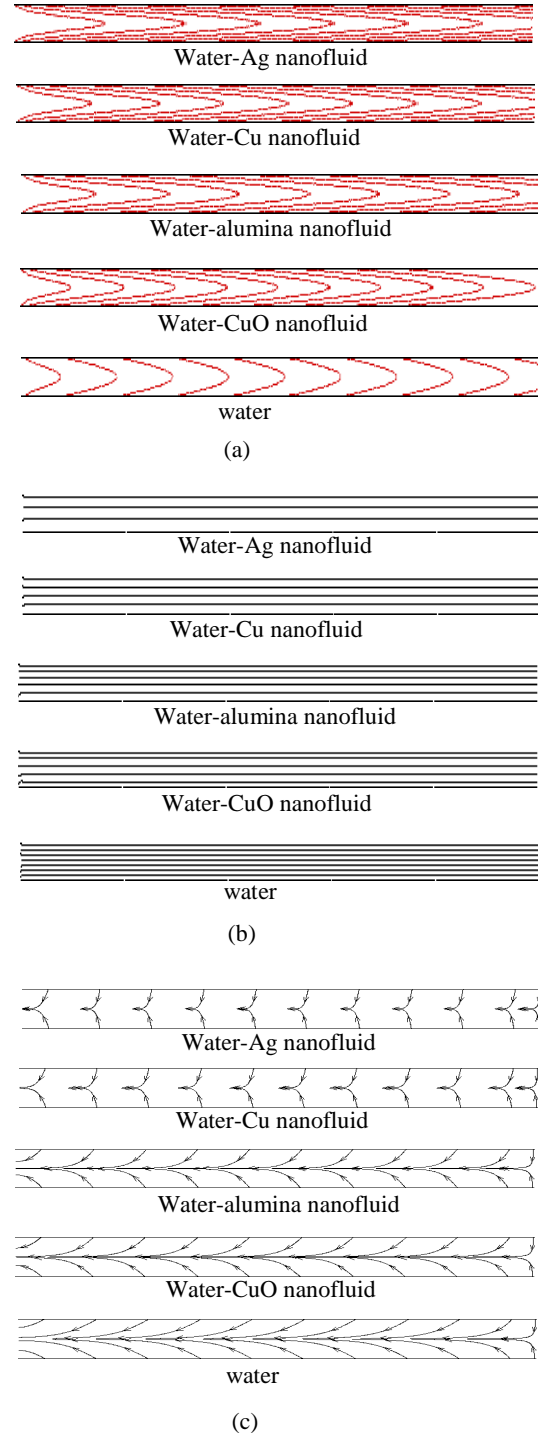

Water-Ag nanofluid

Water-Cu nanofluid

Water-alumina nanofluid

Water-CuO nanofluid

water

(a)

Water-Ag nanofluid

Water-Cu nanofluid

Water-alumina nanofluid

Water-CuO nanofluid

water

(b)

Water-Ag nanofluid

Water-Cu nanofluid

Water-alumina nanofluid

Water-CuO nanofluid

water

(c)

Fig. 6. Effects of various nanofluids as well as base fluid on (a) temperature and (b) streamfunction and (c) heat function

In the heatfunction (Fig. 6 (c)) heatlines are smooth and it is observed that the lines are perfectly

perpendicular to the isotherm lines and the upper and lower walls. This further indicates that the heat flow is conduction dominant. An important point to note is that the heatlines with greater strength become smaller in size at the middle of the flow pipe. This happens due to more conductive heat flux and as we see the case of water, the strength of heatlines go to low. This means that major amount of heat flux or transport occurs for water-silver nanofluid. Thus, relatively less heat flow occurs for clear water.

5.3 Mid-height Temperature

The temperature (dimensional) of water-alumina/copper nanofluid and water-copper nanofluid at the middle height of the riser pipe with the influences of solid volume fraction are displayed in Fig. 7(i) and (ii) respectively. From the Fig. 7(i) it is shown that the inlet temperature of fluid is maintained at 300K and then it increases gradually with the contact of heated solid upper and lower boundaries of the riser pipe. And finally the output temperature of water-alumina/copper nanofluid becomes 344K, 350K, 354K, 357K, 357K and 357K for ϕ = 0%, 1%, 3%, 5%, 7% and 10% respectively.

Similarly mid-height temperature increases with growing ϕ upto 5% and then remains unchanged. The output temperature of water-Cu nanofluid becomes 344K, 350K, 355K, 360K, 360K and 360K for ϕ = 0%, 1%, 3%, 5%, 7% and 10% respectively.
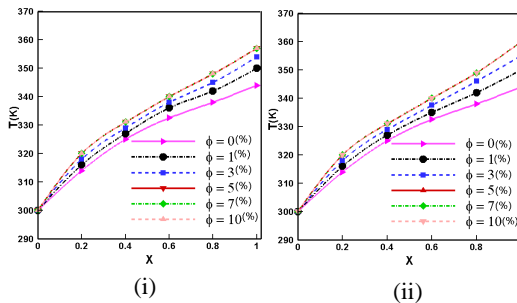

Fig. 7. Mid-height temperature for the effect of (i) water-Al₂O₃/Cu nanofluid and (i) water-Cu nanofluid

5.4 Rate of Heat Transfer

In Fig. 8(i) average Nusselt number at the upper hot surface with various solid volume fraction is accounted for nanofluid having double and single nanoparticle as well as clear water. *Nu* enhances sharply with growing ϕ upto 5% and then remains unchanged for advance mixture of solid volume faction for water based nanofluid having double as well as single nanoparticles. Rate of heat transfer enhances by 27% and 22% with the variation of ϕ from 0% to 5% for water-alumina/copper and water-alumina nanofluids respectively.

From the plot of the average Nusselt number (*Nu*)-solid volume fraction (ϕ) of the Fig. 8(ii) it is observed that rate of heat transfer is maximum for water-Ag nanofluid. And then *Nu* devalues for

water-Cu, water-Al₂O₃, water-CuO nanofluids respectively. Heat transfer rate increases by 33%, 30%, 22% and 20% with the variation of ϕ from 1% to 5% respectively for Ag, Cu, Al₂O₃ and CuO nanoparticles. Here *Nu* remains constant for water with the variation of ϕ. For all nanofluids mean Nusselt number rises sharply from 0% to 5% and heat transfer rate remains nearly constant for escalating ϕ from 5% to 10%. Thus, it is not always beneficial to introduce more solid volume fraction of nanoparticle with base fluid for a flow.
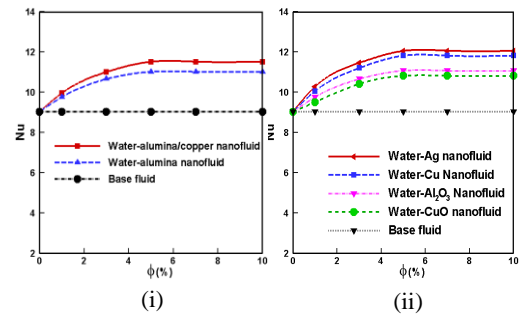

Fig. 8. Mean Nusselt number for the effect of (i) nanofluid with single and double nanoparticles and (i) various nanofluids

5.5 Mean Bulk Temperature

Figures 9(i) and (ii) display mean temperature (θ_{av}) versus the nanofluid with single and double nanoparticles and various nanofluids. θ_{av} grows sequentially for ϕ upto 5% for both figures. Mean temperature remains constant for further increasing values of solid volume fraction. It is well known that thermal conductivity of Ag nanoparticle is higher than others. Higher thermal conductivity is capable to carry more heat. Thus average bulk temperature of water-Al₂O₃/Cu and water-Ag nanofluids have found higher in Figs. 9(i) and 9(ii) respectively. There is no change of water (ϕ = 0%) due to the deviation of nanoparticles volume fraction.
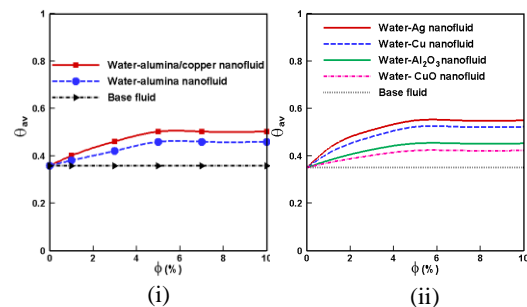

Fig. 9. Average temperature for the effect of (i) nanofluid with single and double nanoparticles and (i) various nanofluids

5.6 Magnitude of Average Velocity

Magnitude of average velocity vector (V_{av}) for the nanofluid with single and double nanoparticles and various nanofluids are expressed in the Fig. 10(i) and (ii). V_{av} has notable changes with different

values of solid concentration of different nanofluids. Growing ϕ devalues mean velocity of the nanofluid through the riser pipe of the flat plate solar collector. Here water-alumina nanofluid has higher mean velocity than the water-alumina/copper nanofluid. Less solid concentrated nanofluid has greater velocity than highly concentrated nanofluid.

Also mean velocity is obtained maximum for water and then for water-alumina, water-copper oxide, water-copper and water-silver nanofluids respectively. Water has lower density than all considered nanofluids.
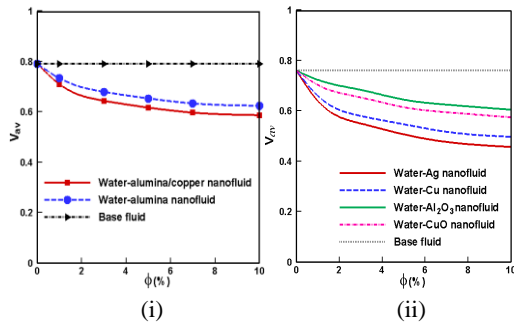

Fig. 10. Mean velocity for the effect of (i) nanofluid with single and double nanoparticles and (i) various nanofluids

5.7 Collector Efficiency

Figures 11(i) and (ii) express the collector efficiency η(%)-solid volume fraction ϕ (%) for the nanofluid with single and double nanoparticles and various nanofluids. Here ϕ varies from 0% to 10%. From this figure it is observed that adding low quantities of nanoparticles leads to the remarkable enhancement of the efficiency until a volume fraction of approximately 5%. After a volume fraction of 5%, the efficiency begins to level off with increasing volume fraction. The authors attribute this unchanging to the high increase of the fluid absorption at high particle loadings. The main difference in the steady-state efficiency occurs in water based nanofluid having alumina and copper nanoparticles. Consequently, percentage of solar collector efficiency is obtained maximum for water-silver nanofluid in Fig. 11(ii). Collector efficiency rises from 65% to 89% with growing the solid volume fraction ϕ from 0% to 5% for water-Ag nanofluid.
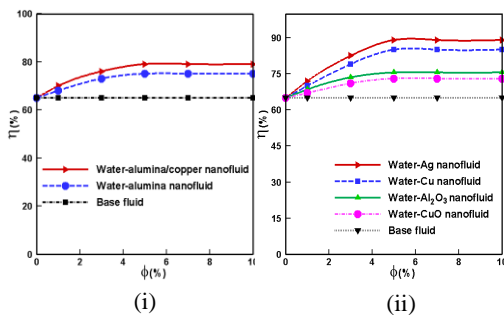

Fig. 11. Collector efficiency for the effect of (i) nanofluid with single and double nanoparticles and (i) various nanofluids

6. Conclusion

The finite element simulation of forced convection heat transfer by a water based nanofluid containing double nanoparticles and various nanofluids inside the riser pipe of a flat plate solar collector is accounted. Various solid volume fraction ($\phi = \phi_1 + \phi_2$) of water-Al_2O_3/Cu nanofluid and also different nanofluids have been considered for showing the temperature, flow and heat flux patterns. The results of the numerical analysis lead to the following conclusions:

- The structure of the fluid isotherms, streamlines and heatlines through the solar collector is found to appreciably depend upon the $\phi (= \phi_1 + \phi_2)$ and different nanofluids.

- Adding two nanoparticles with base fluid is more effective in enhancing performance of heat loss rate than single nanoparticle.

- Water-Ag nanofluid is better than other considered nanofluids for heat transfer characteristics.

- Percentage of collector efficiency is obtained maximum for 5% solid volume fraction of water-silver nanofluid.

- Mean temperature is higher for nanofluid with double nanoparticles than nanofluid with single nanoparticle.

- Average velocity decreases due to growing ϕ for all nanofluids.

- The mid height temperature of nanofluids increase steadily while passing through the riser pipe for all ϕ.

Thus water-Cu nanofluid is more effective in order to promote heat loss system through the riser pipe of a flat plate solar collector for lower cost of Cu nanoparticles than that of silver nanoparticles.

REFERENCES

Álvarez, A., M.C. Muñiz, L.M. Varela, O. Cabeza (2010), Finite element modelling of a solar collector, *Int. Conf. on Renew. Energies and Power Quality*, Granada (Spain).

Amrutkar, S.K., S. Ghodke, Dr.K.N. Patil, (2012), Solar flat plate collector analysis, *IOSR J. of Engg.*, 2(2), 207-213.

Azad, E. (2009), Interconnected heat pipe solar collector, *IJE Transactions A: Basics*, 22(3), 233.

Chabane, F., N. Moummi, S. Benramache, D. Bensahal, O. Belahssen, F.Z. Lemmadi (2013), Thermal performance optimization of a flat plate solar air heater, *Int. J. of Energy & Tech.*, 5(8), 1–6.

Dara, J.E., K.O. Ikebudu, N.O. Ubani, C.E. Chinwuko, O.A. Ubachukwu (2013),

Evaluation of a passive flat-plate solar collector, *Int. J. of Advancements in Res. & Tech.*, 2(1).

Dechaumphai, P. (1999), Finite Element Method in Engineering. 2nd ed., Chulalongkorn University Press, Bangkok.

Ghasemi, J., S.E. Razavi (2013), Numerical Nanofluid Simulation with Finite Volume Lattice-Boltzmann Enhanced Approach, *J. of Appl. Fluid Mech.*, 6(4), 519-527.

Habib, H.M. and E. R. El-Zahar (2013), Mathematical modeling of heat-transfer for a moving sheet in a moving fluid, *J. of Appl. Fluid Mech.*, 6(3), 369-373.

Iordanou, G. (2009), Flat-plate solar collectors for water heating with improved heat transfer for application in climatic conditions of the mediterranean region, Doctoral thesis, Durham University.

Kalogirou, S.A. (2004), Solar thermal collectors and applications, *Progress in Energy and Combustion Science*, 30, 231–295.

Karanth, K.V., M.S. Manjunath, N.Y. Sharma (2011), Numerical simulation of a solar flat plate collector using discrete transfer radiation model (DTRM)–a CFD approach, *Proc. of the World Congress on Engg., III, WCE 2011*, London, U.K.

Karuppa, R.R.T., P. Pavan and D.R. Rajeev (2012), Experimental investigation of a new solar flat plate collector, *Research J. of Engg. Sciences*, 1(4), 1-8.

Kazeminejad, H. (2002), Numerical analysis of two dimensional parallel flow flat-plate solar collector, *Renew. Energy*, 26, 309–323.

Kolb, A., ERF Winter, R. Viskanta (1999), Experimental studies on a solar air collector with metal matrix absorber, *Solar Energy*, 65(2), 91–98.

Kumar, H (2013), Radiative heat transfer with MHD free convection flow over a stretching porous sheet in presence of heat source subjected to power law heat flux, *J. of Appl. Fluid Mech.*, 6(4), 563-569.

Lambert, A.A., S. Cuevas, J.A. del Rı́o (2006), Enhanced heat transfer using oscillatory flows in solar collectors, *Solar Energy*, 80, 1296–1302.

Lund, K.O. (1986), General thermal analysis of parallel-flow flat-plate solar collector absorbers, *Solar Energy*, 5, 443.

Mahian, O., A. Kianifar, S.A. Kalogirou, I. Pop, S. Wongwises (2013), A review of the applications of nanofluids in solar energy, *Int. J. of Heat and Mass Trans.*, 57, 582–594.

Martín, R.H., A.G. Pinar, J.P. García (2011), Experimental heat transfer research in enhanced flat-plate solar collectors, *Solar Thermal Applications, World Renewable Energy Congress*, 3844-3851.

Maxwell-Garnett, J.C. (1904) Colours in metal glasses and in metallic films, *Philos. Trans. Roy. Soc. A* 203, 385–420.

Nag, A., D. Misra, K.E. De, A. Bhattacharya, S.K. Saha (1989), Parametric study of parallel flow flat plate solar collector using finite element method, *In: Num. Methods in Therm. Problems, Proc. of the 6th Int. Conf.*, Swansea, UK.

Nasrin, R. and M.A. Alim (2013), Free convective analysis in a solar collector using nanofluid, *Engineering e Transaction,* 8(1), 19-27.

Natarajan, E. & R. Sathish (2009), Role of nanofluids in solar water heater, *Int. J. Adv. Manuf. Techno.*, DOI 10.1007/s00170-008-1876-8.

Ogut, E.B. (2009), Natural convection of water-based nanofluids in an inclined enclosure with a heat source, *Int. J. of Thermal Sciences*, 48(11), 2063-2073.

Otanicar, T.P., P.E. Phelan, R.S. Prasher, G. Rosengarten, and R.A. Taylor (2010), Nanofluid-based direct absorption solar collector, *J. of Renew. and Sustainable Energy*, 2, 033102.

Pak, B.C., Y. Cho (1998), Hydrodynamic and heat transfer study of dispersed fluids with submicron metallic oxide particle, *Experimental Heat Trans.*, 11, 151-170.

Patil, M., P. G. Hegde and K. N. Seetharamu (2013), Effects of radiation and cold wall temperature boundary conditions on natural convection in a vertical annular porous medium, *J. of Appl. Fluid Mech.*, 6(2), 177-189.

Piao, Y., EG. Hauptmann, M. Iqbal (1994), Forced convective heat transfer in cross-corrugated solar air heaters, *ASME J. of Solar Energy Engg.*, 116, 212-214.

Polvongsri, S. and T. Kiatsiriroat (2011), Enhancement of Flat-Plate Solar Collector

Thermal Performance with Silver Nano-fluid, *The 2nd TSME Int. Conf. on Mech. Engg.*, Krabi.

Rao, V.S., L. A. Babu and R. S. Raju (2013), Finite element analysis of radiation and mass transfer flow past semi- infinite moving vertical plate with viscous dissipation, *J. of Appl. Fluid Mech.*, 6(3), 321-329.

Saleh, A.M. (2012), Modeling of flat-plate solar collector operation in transient states, thesis of Master of Sci. in Engg., Purdue University, Fort Wayne, Indiana.

Saleh, H., R. Roslan, I. Hashim (2011), Natural convection heat transfer in a nanofluid-filled trapezoidal enclosure. *Int. J. of Heat and Mass Trans.,* 54, 194–201.

Sandhu, G. (2013), *Experimental study of temperature field in flat-plate collector and heat transfer enhancement with the use of insert devices*, (M. of Engg. Sci. theseis), The School of Graduate and Postdoctoral Studies, The University of Western Ontario London, Ontario, Canada.

Singh, O.P., M. Garg, V. Kumar and Y. V. Chaudhary (2013), Effect of cooling system design on engine oil temperature, *J. of Appl. Fluid Mech.*, 6(1), 61-71.

Struckmann, F. (2008), Analysis of a Flat-plate Solar Collector, *Project Report 2008 MVK160 Heat and Mass Transport*, Lund, Sweden.

Taylor, C., P. Hood (1973), A numerical solution of the Navier-Stokes equations using finite element technique. *Computer and Fluids*, 1, 73–89.

Taylor, R.A., P.E. Phelan, T.P. Otanicar, R. Adrian, R. Prasher (2011), Nanofluid optical property characterization: towards efficient direct absorption solar collectors, *Nanoscale Research Letters*, 6, 225.

Tripanagnostopoulos, Y., M. Souliotis, T. Nousia (2000), Solar collectors with colored absorbers, *Solar Energy*, 68, 343–356.

Tyagi, H., P. Phelan, R. Prasher (2009), Predicted efficiency of a low-temperature nanofluid-based direct absorption solar collector, *J. of Solar Energy Engg.*, 131/041004-1.

Zambolin, E. (2011), Theoretical and experimental study of solar thermal collector systems and components, Scuola di Dottorato di Ricerca in Ingegneria Industriale, Indirizzo Fisica Tecnica.

Zienkiewicz, O.C. and Taylor, R.L. (1991), The finite element method, Fourth Ed., McGraw-Hill.